Insights into the structure of the stable and metastable $(GeTe)_m(Sb_2Te_3)_n$ compounds

Juarez L. F. Da Silva,[1] Aron Walsh,[1] and Hosun Lee[2]
[1]*National Renewable Energy Laboratory, 1617 Cole Boulevard, Golden, Colorado 80401, USA*
[2]*Department of Applied Physics, Kyung Hee University, Suwon 446-701, Republic of Korea*
(Received 5 September 2008; published 30 December 2008)

Using first-principles calculations, we identify the mechanisms that lead to the lowest energy structures for the stable and metastable $(GeTe)_m(Sb_2Te_3)_n$ (GST) compounds, namely, strain energy release by the formation of superlattice structures along of the hexagonal [0001] direction and by maximizing the number of Te atoms surrounded by three Ge and three Sb atoms (3Ge-Te-3Sb rule) and Peierls-type bond dimerization. The intrinsic vacancies form ordered planes perpendicular to the stacking direction in both phases, which separate the GST building blocks. The 3Ge-Te-3Sb rule leads to the intermixing of Ge and Sb atoms in the (0001) planes for $Ge_3Sb_2Te_6$ and $Ge_2Sb_2Te_5$, while only single atomic species in the (0001) planes satisfy this rule for the $GeSb_2Te_4$ and $GeSb_4Te_7$ compositions. Furthermore, we explain the volume expansion of the metastable phase with respect to the stable phase as a consequence of the different stacking sequence of the Te atoms in the stable and metastable phases, which leads to a smaller Coulomb repulsion in the stable phase. The calculated equilibrium lattice parameters are in excellent agreement with experimental results and differ by less than 1% from the lattice parameters derived from a combination of the GeTe and Sb_2Te_3 parent compounds.

DOI: 10.1103/PhysRevB.78.224111 PACS number(s): 61.50.−f, 63.20.dk, 63.22.Np

I. INTRODUCTION

Phase-change materials such as the ternary $(GeTe)_m(Sb_2Te_3)_n$ (GST) compounds have been considered as one of the most natural candidates for the development of nonvolatile memory devices.[1,2] This expectation is based on the current applications of GST compounds in optical storage products, namely, rewritable compact disks (CD-RW), digital versatile disks (DVDs), and blu-ray disks (BDs), which rely on a fast and reversible resistance change between a metastable crystalline phase (low resistivity) and an amorphous phase (high resistivity).[2,3] The GST compounds are widely employed in rewritable multimedia technology, however, their success as a candidate for nonvolatile memory devices requires a complete understanding of the basic properties of the GST phases involved in the transition, which can be used to improve the transition speed as well as the reversibility between the metastable crystalline and amorphous phases. Several recent studies have focused on the characterization of the amorphous phase,[2,4–11] however, as we will show below, there is no common consensus on the crystalline structure of the GST compounds, which plays an important role in the phase transition to the amorphous phase.

The ternary GST compounds have two crystalline polymorphs, namely, a ground-state phase and a slightly higher energy metastable phase. X-ray diffraction (XRD) studies[12–20] observed that the stable GST phase for different compositions crystallize in hexagonal structures ($P\bar{3}m1$ or $R\bar{3}m$), in which the Ge, Sb, and Te atoms form building blocks composed of 1 f.u. stacked along the [0001] direction (c axis). The building blocks are separated by intrinsic vacancies originating from Sb_2Te_3, in which they are naturally present (see Fig. 1), and hence, there is a large separation between the GST blocks, e.g., from 3.9 to 4.5 Å. Thus, the structure of the stable phase appears well defined, however, there is a debate related with the occupation of the cation sites by Ge and Sb atoms in the hexagonal lattices ($P\bar{3}m1$ or $R\bar{3}m$). For example, Matsunaga and co-workers[17–20] using XRD suggested that the cation planes perpendicular to the stacking [0001] direction contain both species (Ge and Sb), however, Kooi and De Hosson[16] also using XRD suggested that each cation plane contain only one species, i.e., Ge or Sb (see Fig. 2). Recent first-principles calculations[21,22] for four GST compositions support the XRD results obtained by Kooi

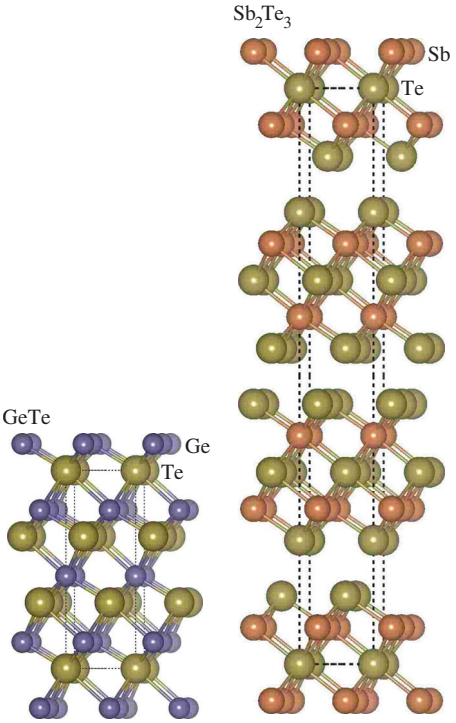

FIG. 1. (Color online) Crystal structures of the bulk GeTe and Sb_2Te_3 in the conventional hexagonal unit cells, which contain 3 f.u. The primitive rhombohedral unit cell contains 1 f.u. The Ge (small balls), Sb (medium balls), and Te (large balls) are labeled, while the dashed lines indicate the conventional hexagonal lattice.

 ©2008 The American Physical Society

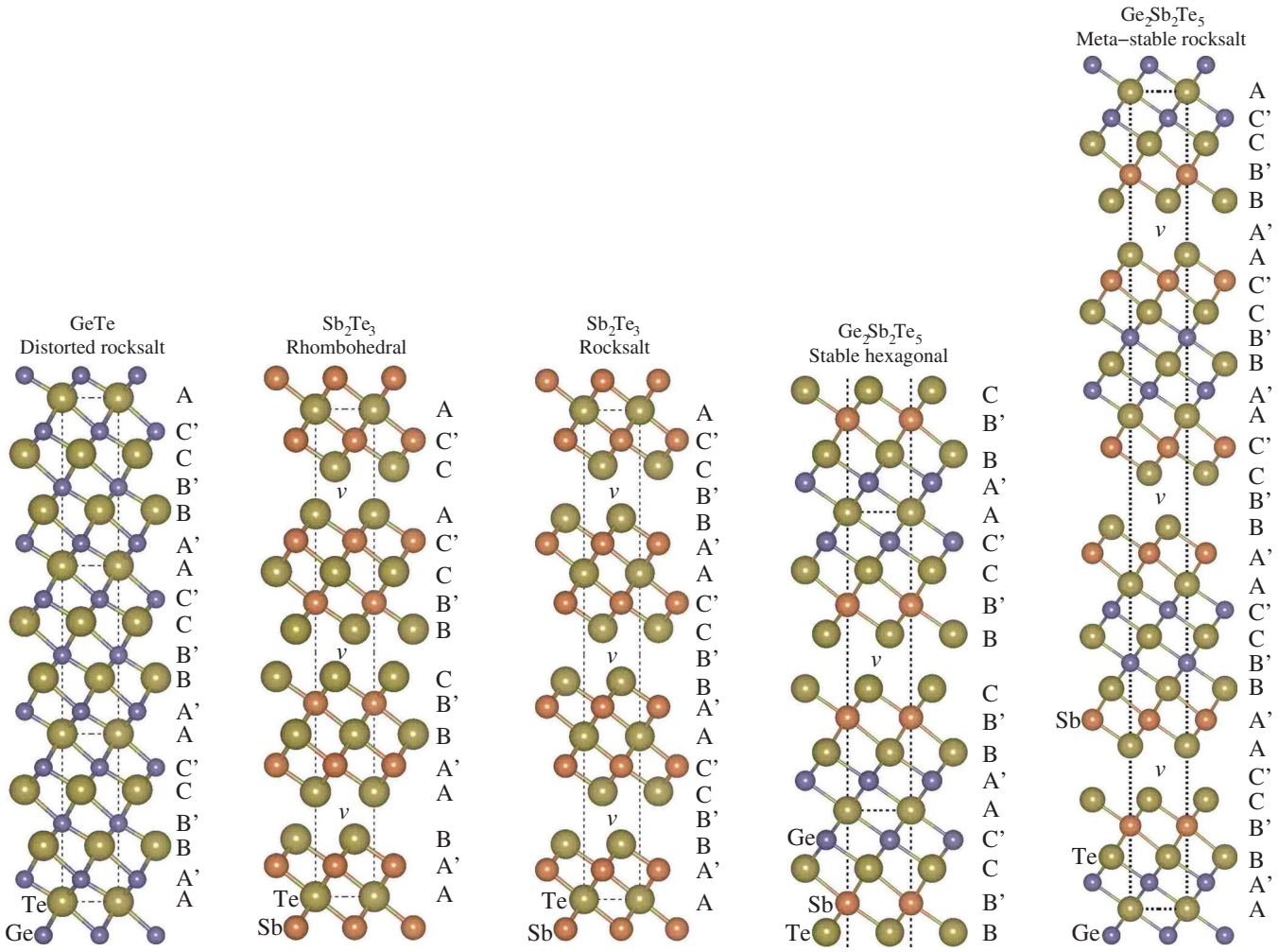

FIG. 2. (Color online) Crystal structures of the bulk GeTe (distorted rocksalt), Sb_2Te_3 (rhombohedral and rocksalt), and $Ge_2Sb_2Te_5$ (stable hexagonal and metastable rocksalt) compounds. All structures are represented in the conventional hexagonal lattices indicated by the dashed lines. *A*, *B*, and *C* indicate stacking sequence and have coordinates $(0,0,z)$, $(2/3,1/3,z)$, and $(1/3,2/3,z)$, respectively, using the $(1\times1\times n)$ unit cell. The Ge (small balls), Sb (medium balls), Te (large balls), and intrinsic vacancies (v) are labeled.

and De Hosson,[16] however, no structure mechanism is provided to justify either of the two suggestions, i.e., a mixed Ge and Sb or single species layer.

High-resolution transmission electron microscopy (HRTEM), XRD, and x-ray absorption fine-structure spectroscopy (EXAFS) studies have suggested that the metastable GST phase crystallizes in a rocksalt-type (RS-type) structure, in which the Te atoms occupy the anion (4*a*-type) sites, whereas the Ge, Sb, and intrinsic vacancies occupy randomly the cation (4*b*-type) sites.[4,23–26] It is important to notice that intrinsic vacancies occupy defined high-symmetry lattice sites in the metastable phase, while they only separate the GST building blocks in the stable phase, which increases the complexity of the metastable RS-type structures. First-principles calculations performed by Sun *et al.*[21] for metastable $Ge_2Sb_2Te_5$ found no intermixing of Ge and Sb atoms in the planes perpendicular to the RS [111] direction ([0001] direction using a hexagonal lattice). Their model, in which the intrinsic vacancies are ordered in planes perpendicular to the RS [111] direction, leads to the formation of Ge-Te bond lengths of 2.99 and 3.03 Å (Δ_b=0.04 Å) in $Ge_2Sb_2Te_5$, however, experimental studies based on EXAFS found bond lengths of 2.83 and 3.15 Å (Δ_b=0.32 Å),[26] which indicates that the structure models suggested by Sun *et al.*[21] cannot provide a reliable description of the experimental trends. First-principles calculations performed by Eom *et al.*[27] suggest that intrinsic vacancies tend to distribute randomly in $Ge_2Sb_2Te_5$, which is in contrast to the results obtained by Sun *et al.*[21] and experimental results based on HRTEM,[25] which indicates intrinsic vacancy ordering. However, we want to point out that Eom *et al.*[27] conclusions were based on calculations for nonstoichiometric composition ($Ge_2Sb_2Te_4$) instead of the stoichiometric $Ge_2Sb_2Te_5$ compound.

Therefore, even though the GST compounds are currently used in rewritable technological applications, the knowledge and understanding of their atomic structure are far from satisfactory. For both crystalline phases, the Te atoms occupy well-defined anion lattice sites, whereas the exact atomic occupations of Ge, Sb, and intrinsic vacancies (metastable) have been a source of controversy and debate. In the present work, we will show that those controversies can be resolved through identification of the underlying structure formation

mechanisms that leads to the lowest energy structures, as well as the relation between the parent GeTe and Sb_2Te_3 compounds and the GST compounds. In order to achieve these goals, we performed first-principles density-functional theory (DFT) calculations for the GST compounds as a function of Ge/Sb composition, namely, $Ge_3Sb_3Te_6$, $Ge_2Sb_2Te_5$, $GeSb_2Te_4$, $GeSb_4Te_7$, as well as for the single GeTe and Sb_2Te_3 compounds. Based on our calculations and analysis, we identified a set of basic rules that lead to the lowest energy structures, which explain the two Ge-Te bond lengths in GST compounds, and the volume expansion of the metastable phase compared with the stable phase.

The remainder of this paper is organized as follows. In Sec. II, we report the theoretical approach and computational details, while in Secs. III and IV we discuss the structures of GeTe and Sb_2Te_3. In Sec. V, we discuss the structural similarities between both single compounds and explore the lowest energy GST structures. Finally, in the Appendix, we discuss the accuracy of our results.

II. THEORETICAL APPROACH AND COMPUTATIONAL DETAILS

Our first-principles calculations are based on the all-electron projector augmented wave (PAW) method[28,29] and DFT within the generalized gradient approximation Perdew-Burke-Ernzerhof (GGA-PBE) (Ref. 30) as implemented in VASP.[31,32] For total-energy and stress tensor calculations, we employed cutoff energies of 288 and 576 eV, respectively. For the Brillouin-zone integration a $(6\times6\times1)$ **k**-point grid was used for bulk $GeSb_2Te_4$ in the conventional hexagonal $(1\times1\times1)$ structure. The same **k**-point density was employed in all other calculations. The total energies and equilibrium volumes at zero temperature for all structures were obtained by full relaxation of the volume, shape, and atomic positions of the unit cell to minimize the quantum-mechanical stresses and forces. In order to check the quality of our results, we calculated the lattice constants using stress tensor as a function of the cutoff energy and number of **k** points in the irreducible part of the Brillouin zone, which are summarized in the Appendix. From those test calculations, we found that a higher cutoff energy (864 eV) and high **k**-point density $(12\times12\times1)$ change a_0 and c_0 by less than 0.10% and 0.35%, respectively.

III. RESULTS AND DISCUSSION

A. Bulk GeTe

At ambient pressure and room temperature (RT), GeTe crystallizes in the distorted RS structure, which has space group $R3m$ and 1 f.u. per primitive rhombohedral unit cell (3 f.u. in the conventional hexagonal unit cell, see Fig. 1).[23,33–35] The anion sites occupied by Te atoms have *ABCABC* stacking along of the RS [111] direction, i.e., [0001] direction in the conventional hexagonal unit cell (see Fig. 2). The distortion occurs along the RS [111] direction, which induces the formation of distorted octahedrons in which each Te atom is surrounded by three Ge at 2.85 Å and three Ge at 3.26 Å, which is consistent with EXAFS results (2.80 and 3.13 Å).[26,36] In the hexagonal lattice configuration as shown in Fig. 1, the lattice parameters are $a_0=4.23$ Å and $c_0/3=3.64$ Å, while the experimental results are 4.17 and 3.54 Å, respectively,[23] i.e., deviations of 1.43% and 2.82%. Furthermore, we obtained a rhombohedral angle of 57.69°, while the experimental value is 58.36°,[23] i.e., a deviation of 1.15%. For temperatures higher than RT, the rhombohedral angle increases and reaches 60° at 716 K (transition temperature),[34] which corresponds to the perfect RS structure. Thus, the structural GeTe parameters are in good agreement with experimental results,[23,34] as well as previous first-principles calculations.[37]

The distortion gives rise to the formation of a sequence of short and long bonds projected along the c axis in Fig. 1 and the formation of a dipole moment along of the c axis.[38] The short and long bond-length sequences can be explained by a Peierls-type electronic instability.[39–41] For the undistorted RS structure, the symmetry of the valence and conduction-band extrema are L_1 and L_2', respectively. Atomic displacement along the RS [111] direction reduces these states both to L_1 symmetry,[42] which can subsequently couple, thus lowering the electronic energy (44 meV/atom) and further increasing the band gap from 0.37 eV (undistorted RS) to 0.50 eV (distorted RS).

B. Bulk Sb_2Te_3

Sb_2Te_3 crystallizes in a rhombohedral layered structure with space group $R\bar{3}m$ with 1 f.u./unit cell, in which the building blocks (Te-Sb-Te-Sb-Te) are stacked along of the [0001] direction in the conventional hexagonal lattice (see Fig. 1).[15,43,44] We observe that a single building block has a RS-type structure, in which the Te atoms within the block have a stacking sequence like in the GeTe structure (*ABC*), however, in the hexagonal unit cell composed of three building blocks the Te atoms have a stacking sequence like *ABCBCACAB* along of the c axis (see Fig. 2). The Sb and Te atoms in the center of the building block are sixfold coordinated, whereas the Te at the edge of the blocks bind only to three Sb atoms within the block. Due to the large interlayer separation between the blocks (3.04 Å) compared with the Sb-Te interlayer distances (1.71 and 1.99 Å), the Sb_2Te_3 structure can be viewed as a composition of Sb, Te, and intrinsic vacancies ordered in the planes perpendicular to the c axis. The existence of the intrinsic vacancy layer is a consequence of the valence of the Sb (V) and Te (VI) atoms and the electron octet counting rule.

The calculated lattice parameters are $a_0=4.34$ Å and $c_0/3=10.43$ Å, which deviate by 1.88% and 2.76% from the experimental results ($a_0=4.26$ Å and $c_0/3=10.15$ Å),[15,44] which are typical error bars for DFT-GGA calculations.[45–47] Furthermore, our results are consistent with previous first-principles calculations ($a_0=8.35$ Å, $c_0=10.28$ Å).[48] Similar to the GeTe structure, there are short (3.03 Å) and long (3.20 Å) bonds in the Sb_2Te_3 structure, however, they are associated with the internal and block edge Te atoms, respectively. We found an energy gain of 32 meV/atom due to the alternating bond lengths, which is smaller than 44 meV/atom in GeTe. Such differences are consistent with the difference

between the short and long bond lengths, e.g., 13.7% for Ge-Te and 5.3% for Sb-Te.

For comparison, we calculated Sb_2Te_3 also in the RS structure (see Fig. 2), in which the Te atoms are stacked along of the RS [111] direction ([0001] direction in the hexagonal cell) like in GeTe (*ABCABCABC*). Thus, the intrinsic vacancies occupy the cation sites. We found that Sb_2Te_3 in the RS-type structure is only 15 meV/f.u. higher in energy than the rhombohedral structure, which is expected by taking into account that all structural features observed in the rhombohedral structure such as short and long bond lengths and intrinsic vacancy ordering are replicated in the RS-type structure, except for the stacking sequence.

C. Stable and metastable GeTe-Sb_2Te_3 phases

As mentioned in Sec. I, the stable and metastable GST phases indicate GST compounds within hexagonal ($P\bar{3}m1$ or $R\bar{3}m$) and RS-type structures, respectively. These have a large number of similarities and both can be represented using hexagonal lattices with the Ge, Sb, Te, and intrinsic vacancies stacked along of the *c* axis (Fig. 2).

1. GeTe and Sb_2Te_3 structure similarities

GeTe and Sb_2Te_3 share a large number of structural similarities. For example, the stacking sequence of Te in GeTe is *ABC* along of the [0001] direction, whereas in Sb_2Te_3 it is *ABCBCACAB* (rhombohedral) and *ABCABCABC* (RS type). Thus, there is a direct connection with the stacking sequence in the GST phases. For example, in the stable GST phase, x-ray diffraction studies[12,13,16–20] obtained stacking sequences for the Te atoms along of the [0001] direction such as *ABCACABCABABCABCBC*, *ABCBC*, *ABCBCABABCAC*, and *ABCACAB* for $Ge_3Sb_2Te_6$, $Ge_2Sb_2Te_5$, $GeSb_2Te_4$, and $GeSb_4Te_7$, respectively. However, in the metastable phase, which crystallizes in a RS-type structure,[4,23–25] the Te atoms stacked along of the RS [111] direction have a stacking such as *ABCABCABCABC* for all compositions (see Fig. 2). The number of Te layers in the hexagonal cells depends on the stacking and number of GeTe and Sb_2Te_3 units in the $(GeTe)_m(Sb_2Te_3)_n$ compound. Thus, this analysis indicates that Sb_2Te_3 plays an important role in the Te stacking sequence of the GST phases, i.e., it dictates the stacking in the stable and metastable GST phases.

The lattice parameters, a_0^{GeTe} and $a_0^{Sb_2Te_3}$, differ by less than 2.2%, which indicates a very small mismatch between the two hexagonal lattices. Furthermore, using the lattice constants (a_0 and c_0) of GeTe (distorted RS) and Sb_2Te_3 (RS type), we derived averaged lattice constants for the conventional RS structure, e.g., $a_0^{RS}(GeTe)=(a_0^{GeTe}\sqrt{2}+c_0^{GeTe}\sqrt{3})/2$. We found $a_0^{RS}=6.14$ and 6.20 Å for GeTe and Sb_2Te_3, i.e., a difference of less than 1.0% between the average RS lattice constants, which is unexpected taking into account that Ge and Sb have different valences, however, the valence difference is compensated by the presence of intrinsic vacancies in the Sb_2Te_3 structures. Thus, the average lattice constants of GST compounds in the metastable phase should not differ significantly, which is consistent with experimental results,[17,18,23,24] as well as our calculations (see below).

2. GST structure mechanisms

Based on the structural similarities between GeTe and Sb_2Te_3, experimental studies for the GST phases,[12,13,16–20,23–25] as well as previous first-principles calculations,[21,49,50] it is natural to consider the stoichiometric GST compounds in both phases as superlattices of GeTe and Sb_2Te_3 in which the stacking sequences are dictated by the Sb_2Te_3 structures. Therefore, in order to calculate GST in both crystalline phases and at different Ge/Sb compositions, which is the key to obtain an atom-level understanding of the structure mechanism that drives the formation of the those superlattice structures, we employed a set of well defined steps. (i) Both GST phases are described using $(2\times2\times1)$ hexagonal superlattices, in which the number of f.u. within the hexagonal unit cell depends on the $(GeTe)_m(Sb_2Te_3)_n$ composition and phase. (ii) The stacking sequence of the Te atoms in both phases is determined by the stacking of the Te atoms in the rhombohedral and RS-type Sb_2Te_3 structures and the number of $(GeTe)_m(Sb_2Te_3)_n$ units. As mentioned before, in the metastable phase intrinsic vacancies occupy cation sites together with the Ge and Sb atoms, however, in the stable phase, the intrinsic vacancies do not occupy high-symmetry sites but only separate the building blocks as in the rhombohedral Sb_2Te_3 structure. (iii) For both GST phases we considered different Ge, Sb, and Te sequences along of the *c* axis, e.g., Ge atoms located near to the intrinsic vacancy regions instead of Sb atoms, occupation of the *A*, *B*, and *C* sites by Ge or Sb atoms. (iv) For both phases, we considered model structures in which the Ge and Sb atoms form pure planes perpendicular to the *c* axis or intermixed planes, in which there are Ge and Sb atoms at different compositions, e.g., 25% (Ge) and 75% (Sb), 50% (Ge) and 50% (Sb), and 75% (Ge) and 25% (Sb). (v) For the metastable GST phase, we considered ordered (perpendicular to the *c* axis) and random occupations of the cation sites by intrinsic vacancies. (vi) For all calculated systems, the lattice parameters a_0 and c_0 are relaxed independently.

Therefore, all calculated structure models (about 100) were based on physical arguments instead of a random search in the configurational space of the atomic positions and lattice vectors,[51] which is not possible to be applied using first-principles calculations for systems containing about 100–150 atoms even using large-scale supercomputers. The approach adopted in this work was successfully employed to study the multilayered *M*-modulated $InMO_3(ZnO)_n$ compounds (M=In, Ga, Al and n is an integer).[52] The lowest energy GST structures are shown in Figs. 3 and 4, while the structural parameters of the lowest energy structures are summarized in Tables I and II.

From our calculations and analysis, we identified a set of rules and formation mechanisms that lead to the lowest energy structures, which will be explained below using the lowest energy structures shown in Figs. 3 and 4 as examples, as well as the structures shown in Fig. 2. (i) For both GST phases, the $(GeTe)_m(Sb_2Te_3)_n$ superlattices are constructed by the insertion of *m*GeTe units into one single Sb_2Te_3 build-

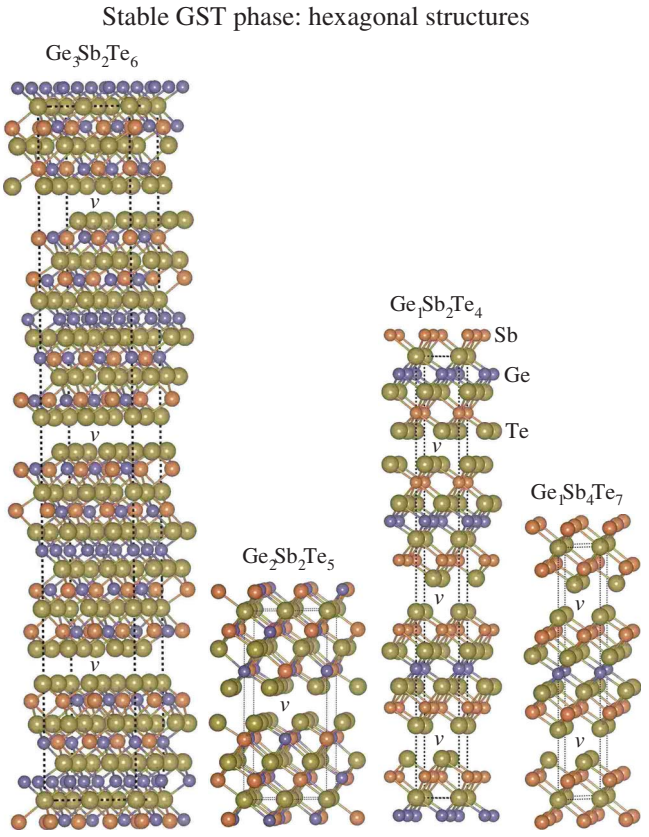

FIG. 3. (Color online) Lowest energy structures for the stable GST phase, namely, for $Ge_3Sb_2Te_6$, $Ge_2Sb_2Te_5$, $GeSb_2Te_4$, and $GeSb_4Te_7$, in which there are 12, 4, 3, and 1 f.u. within the indicated hexagonal unit cells (dashed lines). The Ge (small balls), Sb (medium balls), Te (large balls), and intrinsic vacancies (v) are indicated.

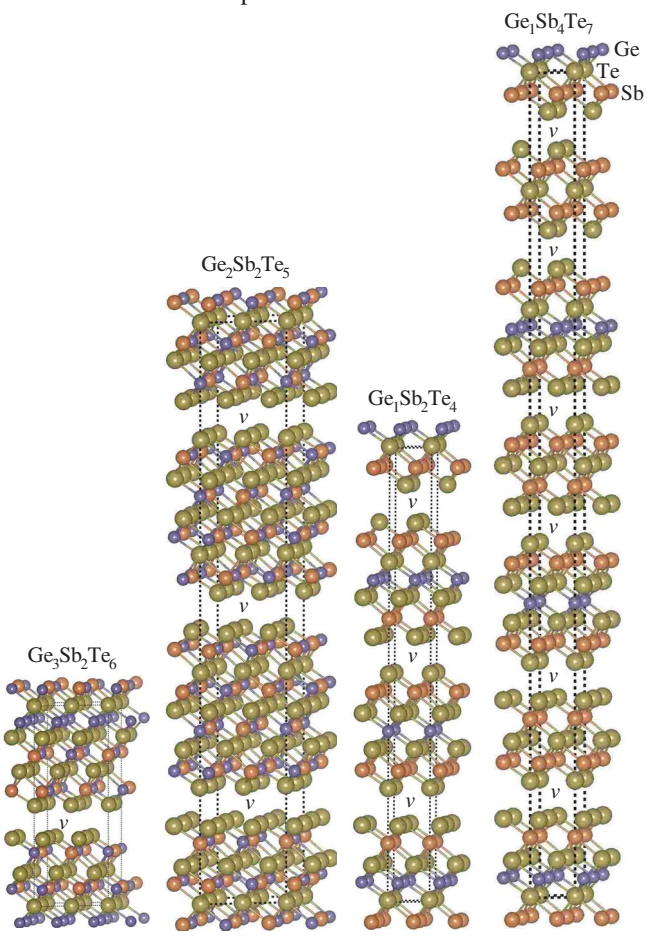

FIG. 4. (Color online) Lowest energy structures for the metastable GST phase, namely, for $Ge_3Sb_2Te_6$, $Ge_2Sb_2Te_5$, $GeSb_2Te_4$, and $GeSb_4Te_7$, in which there are 4, 12, 3, and 3 f.u. within the indicated hexagonal unit cells (dashed lines). The Ge (small balls), Sb (medium balls), Te (large balls), and intrinsic vacancies (v) are indicated.

ing block (Te-Sb-Te-Sb-Te), while the remaining $(n-1)Sb_2Te_3$ units form $(n-1)Sb_2Te_3$ blocks as in the original Sb_2Te_3 parent structure, i.e.,

$$(GeTe)_m(Sb_2Te_3)_n = [(GeTe)_m(Sb_2Te_3)] + [(n-1)Sb_2Te_3].$$

This superlattice configuration is expected as the GST system tends to preserve as much as possible the parent structures which are optimized based on the atomic sizes and valences of the Ge, Sb, and Te atoms. For example, in the lowest energy $GeSb_4Te_7$ structure, one unit of GeTe is inserted into a single Sb_2Te_3 block, while the second block is preserved as in the original Sb_2Te_3 structure. This rule is also satisfied by all reported experimental structures beyond those studied in the present work.[12,13,16–20] For example, Matsunaga *et al.*[20] found using x-ray diffraction that six GeTe units are inserted within a single Sb_2Te_3 block in the $Ge_6Sb_2T_9$ compound. (ii) In the resulting $(GeTe)_m(Sb_2Te_3)$ building blocks, Ge atoms locate preferentially at the center of the block, while the Sb atoms locate preferentially close to the edges, in which the undercoordinated Te atoms are located. These preferences are due to different valence of Ge (IV) and Sb (V), as well as to the smaller size of the Ge atoms, e.g., calculated covalent radius using bulk Ge and Sb yields 1.25 and 1.48 Å for Ge and Sb, respectively. This rule is satisfied in all recent experimental studies,[16–20] as well as previous first-principles calculations.[21,22,50] (iii) We found that the strain energy of the crystal can be further reduced by an interchange of Ge and Sb atoms between different layers to maximize the number of Te atoms surrounded by three Ge and three Sb (3Ge-Te-3Sb), in which the Ge and Sb locate at the opposite corners of the octahedron structures. This gives rise to the formation of a sequence of short and long lengths as in the GeTe and Sb_2Te_3 structures, i.e., the Peierls-type electronic instability plays an important role. This rule is supported by experimental results. For example, using a single species (Ge or Sb) per plane for $Ge_2Sb_2Te_5$ (see Fig. 2), which does not satisfy this rule, we found bond lengths of 2.99 and 3.03 Å (Δ_b=0.04 Å) for Ge-Te, while EXAFS studies obtained 2.83 and 3.15 Å (Δ_b=0.32 Å),[26] i.e., it cannot explain the experimental results. However, structure models for $Ge_2Sb_2Te_5$, which satisfy the (3Ge-Te-3Sb) rule, yield bond lengths of 2.87 and 3.24 Å (Δ_b=0.37 Å) for Ge-Te, which are consistent with the experimental results. Furthermore, structure models for $GeSb_2Te_4$ employing the (3Ge-Te-3Sb) rule yields only a single bond length for

TABLE I. Lattice parameters of the GeTe, GST, and Sb_2Te_3 compounds. a_0 is given per $(1\times1\times1)$ unit cell, while c_0 is given per number of building blocks in the $(1\times1\times1)$ hexagonal cell. The numbers in parentheses are obtained using the lattice constants of GeTe and Sb_2Te_3 (see text). The experimental results for the metastable phase are obtained from the averaged $a_0^{\text{RS type}}$ (see text).

	Stable hexagonal GST structures						Metastable rocksalt GST structures					
	a_0 (Å)			c_0 (Å)			a_0 (Å)			c_0 (Å)		
GeTe	4.23		4.17[a]	3.64		3.54[a]						
$Ge_3Sb_2Te_6$	4.28	(4.26)	4.21[b]	21.15	(21.34)	20.77[b]	4.26	(4.25)		21.65	(21.81)	
$Ge_2Sb_2Te_5$	4.27	(4.26)	4.22[c]	17.89	(17.71)	17.24[c]	4.27	(4.26)	4.26[c]	18.36	(18.17)	17.40[c]
$GeSb_2Te_4$	4.31	(4.28)	4.27[d]	14.04	(14.07)	13.90[d]	4.30	(4.27)	4.27[d]	14.38	(14.53)	13.96[d]
$GeSb_4Te_7$	4.32	(4.30)		24.42	(24.50)		4.30	(4.29)		25.26	(25.42)	
Sb_2Te_3	4.34		4.26[e]	10.43		10.15[e]	4.32			10.89		

[a]Experiment in Ref. 23.
[b]Experiment at 90 K in Ref. 19.
[c]Experiment in Ref. 18.
[d]Experiment at 873 K in Ref. 17.
[e]Experiment in Ref. 44.

Ge-Te, which is also consistent with experimental results.[26] (iv) In the lowest energy metastable GST structures, the intrinsic vacancies form ordered planes perpendicular to the c axis, i.e., (111) planes in the RS-type structure, which is consistent with experimental data obtained by HRTEM.[25] All the metastable structures in which the intrinsic vacancies are randomly distributed among the cation sites have higher energies, e.g., higher by 180–720 meV/f.u. for $Ge_2Sb_2Te_5$. Thus, our results suggest that a random distribution of intrinsic vacancies can be present only in high energy or nonequilibrium structures, which may play an important role in the phase transition from the metastable to the amorphous phase.

3. GST lowest energy structures

Thus, due to the rules summarized above, the lowest energy structures for the studied Ge/Sb compositions show differences concerning the occupation of the cation sites. There are three compositions to consider, namely, $Ge/Sb>1$, $Ge/Sb=1$, and $Ge/Sb<1$. For Ge rich, e.g., $Ge_3Sb_2Te_6$, the Ge and Sb atoms are intermixed in the (0001) planes, however, due to the large number of Ge atoms, not all Te atoms are surrounded by three Ge and three Sb (see Figs. 3 and 4).

TABLE II. Bond lengths (given in Å) of Ge-Te and Sb-Te in the GeTe, GST, and Sb_2Te_3 compounds.

	Stable GST		Metastable GST	
	Ge-Te	Sb-Te	Ge-Te	Sb-Te
GeTe	2.85, 3.26			
$Ge_3Sb_2Te_6$	2.86, 3.23	3.00, 3.29	2.85, 3.24	3.00, 3.39
$Ge_2Sb_2Te_5$	2.87, 3.23	2.97, 3.30	2.87, 3.24	2.96, 3.30
$GeSb_2Te_4$	3.01	3.01, 3.20	3.01	3.01, 3.20
$GeSb_4Te_7$	3.01	3.02, 3.20	3.01	3.02, 3.20
Sb_2Te_3		3.03, 3.20		3.02, 3.20

For $Ge/Sb=1$, e.g., $Ge_2Sb_2Te_5$, all the Te atoms, except the ones at the building block edges, are surrounded by three Ge and three Sb, which, as in the case of $Ge_3Sb_2Te_6$, requires intermixing of Ge and Sb atoms in the same (0001) planes. As discussed above, the intermixing of Ge and Sb atoms in the same planes is essential to explain the different Ge-Te bond lengths in $Ge_2Sb_2Te_5$.[26] Furthermore, it plays an important role in determining the interlayer spacing between the Te planes (see below). For $Ge/Sb<1$ (Ge poor), e.g., $GeSb_2Te_4$ and $GeSb_4Te_7$, we found that only one atomic species (Ge or Sb) per plane satisfy the structure rules for both phases, i.e., no intermixing of Ge and Sb atoms in the (0001) planes is required to satisfy the (3Ge-Te-3Sb) rule. We want to emphasize that all calculated model structures for $GeSb_2Te_4$ and $GeSb_4Te_7$ in which intermixing was allowed have higher energies, e.g., about 20 meV/f.u. for $GeSb_2Te_4$. Our results suggest that the intermixing of Ge and Sb in the planes perpendicular to the c axis is not a rule by itself, but a consequence of the (3Ge-Te-3Sb) rule, which should be taken into account in order to lower the crystal energy of crystalline GST structures.

Our lowest energy structures for $Ge_3Sb_2Te_6$ and $Ge_2Sb_2Te_5$ are consistent with analysis of XRD data, which suggests that the cation sites are occupied by either Ge or Sb atoms in the stable GST phase.[17–19] However, our results do not support the same suggestion for $GeSb_2Te_4$ and $GeSb_4Te_7$,[17] for which we found no intermixing of Ge and Sb atoms in the (0001) planes. Thus, the present results provide important insights, which can be used to improve those XRD model structures. Our results are in contrast to the conclusions obtained by Sun and co-workers[21,22] using first-principles calculations, who found that there is no intermixing of Ge and Sb atoms in the (0001) planes for all studied compositions.

For all GST compositions, the stable phase has lower energy than the metastable phase, however, the relative energies are in the range of a few meV/f.u., e.g., 4.7, 3.6, 2.2, and 28 per f.u. for the $Ge_3Sb_2Te_6$, $Ge_2Sb_2Te_5$, $GeSb_2Te_4$, and

$GeSb_4Te_7$, respectively. This result is expected due to the similar bonding environments but slightly lower Coulomb energy for the stable phase due to the stacking sequence along of the c axis, i.e., it lowers the Coulomb energy by changing the stacking sequence from *ABCABC* (RS, metastable phase) to *ABCBCA* (hexagonal, stable phase). Comparable energy differences (about 15 meV/f.u.) are also obtained between the rhombohedral Sb_2Te_3 and RS-type Sb_2Te_3 structures. This result stresses once more the strong correlation between the Sb_2Te_3 rhombohedral and RS-type structures and the GST structures.

4. GST stability

In order to check the stability of the compounds, we calculated the formation energy, ΔH, with respect to the parents compounds, namely, GeTe and Sb_2Te_3. For example, the formation energy of $(GeTe)_m(Sb_2Te_3)_n$ is given by

$$\Delta H = E_{\text{tot}}^{(\text{GeTe})_m(\text{Sb}_2\text{Te}_3)_n} - mE_{\text{tot}}^{\text{GeTe}} - nE_{\text{tot}}^{\text{Sb}_2\text{Te}_3}, \quad (1)$$

where E_{tot} indicates the total energy per f.u. for the ternary GST compounds, GeTe, and Sb_2Te_3. The formation energies are 72 (77), 26 (29), 12 (14), and 2 meV/f.u. (29 meV/f.u.) for the $Ge_3Sb_2Te_6$, $Ge_2Sb_2Te_5$, $GeSb_2Te_4$, and $GeSb_4Te_7$ in the stable hexagonal phase, respectively. The numbers in parentheses are for the metastable GST phase. We found that the ternary GST compounds are less stable by few meV/f.u. than their separated compounds. We observe that the formation energy increases with the GeTe composition, i.e., these GST structures are less stable, which might play an important role in GST applications.

5. GST equilibrium lattice constants

For both GST phases, we found that the lattice parameters a_0 and c_0 can be calculated in good approximation from the lattice parameters of the separated GeTe and Sb_2Te_3 compounds and their relative compositions in $(GeTe)_m(Sb_2Te_3)_n$. The following equations are used: $a_0^{\text{approx}}=(ma_0^{\text{GeTe}}+na_0^{\text{Sb}_2\text{Te}_3})/(m+n)$ and $c_0^{\text{approx}}=mc_0^{\text{GeTe}}+nc_0^{\text{Sb}_2\text{Te}_3}$, in which the lattice constants of Sb_2Te_3 in the rhombohedral and RS-type structures are used to obtain a_0^{approx} and c_0^{approx} for the stable and metastable GST phases, respectively. The estimated lattice constants are also summarized in Table I. We found that $a_0^{\text{approx}}<a_0$ for all compositions, while $c_0^{\text{approx}}>c_0$ for all compositions, except for $Ge_2Sb_2Te_5$, in which we found that $c_0^{\text{approx}}<c_0$ for both phases. By inspecting the lowest energy structures, we found that the presence of Sb atoms in all cation layers (fully intermixed layers) increases the interlayer separation between Te layers, and hence, it gives rise to a larger c_0 than the sum of the isolated parent compounds in which there is no Ge and Sb intermixing. The same does not occur for $Ge_3Sb_2Te_6$ because the center layer in the building block is composed by only Ge atoms, which disrupt the formation of a sequence of short and long bonds. The approximated lattice constants differ by less than 1.0% compared to the calculated DFT values for the stable and metastable phases. Furthermore, the experimental values (stable phase) can be also derived using the experimental lattice values of GeTe and Sb_2Te_3. Therefore, these results provide strong validation for the superlattice picture introduced above, i.e., there is a direct relation between the lattice constants of GST and the lattice parameters of GeTe and Sb_2Te_3.

For all GST compositions, we found that $c_0^{\text{stable}}<c_0^{\text{metastable}}$ and $a_0^{\text{stable}}\approx a_0^{\text{metastable}}$, which implies that $V_0^{\text{stable}}<V_0^{\text{metastable}}$. These trends are satisfied by DFT calculated lattice parameters as well as by the estimated lattice parameters (a_0^{approx} and c_0^{approx}). Furthermore, we found that $V_0^{\text{rhombohedral}}<V_0^{\text{RS}}$ for Sb_2Te_3. Experimental studies have also obtained the same volume trends, i.e., $V_0^{\text{stable}}<V_0^{\text{metastable}}$,[17,53] which we explain as follows. For all studied compositions, we found that the interlayer separation between the building blocks is smaller in the stable phase (3.0–3.2 Å) than in the metastable phase (3.5–3.7 Å). Due to the RS stacking sequence of the Te atoms in the metastable phase (*ABCABC*), the Te lone pair electrons are oriented toward each other at the block edge, whereas in the stable phase they are not because of a different stacking sequence, e.g., *ABCACAB* for $GeSb_4Te_7$. Therefore the stable phase has lower Coulomb repulsion and shorter Te-Te distances between the blocks, i.e., smaller interlayer separation. For Sb_2Te_3, $Ge_3Sb_2Te_6$, $Ge_2Sb_2Te_5$, $GeSb_2Te_4$, and $GeSb_4Te_7$, the volume expansions are 3.65%, 1.40%, 2.26%, 1.97%, and 2.54%, respectively, while the volume expansions derived from experimental lattice constants are 2.44% (Ref. 53) and 2.83% (Ref. 18) for $Ge_2Sb_2Te_5$ and 0.48% (Ref. 17) for $GeSb_2Te_4$. We want to point out that metastructures in which the intrinsic vacancies are randomly distributed among the cation sites show a volume expansion of 4.0% (averaged over five structures) for $Ge_2Sb_2Te_5$, hence, intrinsic vacancy ordering plays an important role in the volume expansion.

All lattice parameters are in good agreement with experimental results,[17,19] i.e., deviations of about 1.0%–4.0% (see Table I). For the metastable phase, we derived the average RS lattice constant, a_0^{RS}, using our results for a_0 and c_0. We found 6.13, 6.20, 6.15, and 6.17 Å for $Ge_3Sb_2Te_6$, $Ge_2Sb_2Te_5$, $GeSb_2Te_4$, and $GeSb_4Te_7$, respectively, which is consistent with experimental results.[17,18,23,24] For both GST phases, the bond lengths of Ge-Te and Sb-Te show similar trends (see Table II), which are consistent with EXAFS analysis.[26] We found two bond lengths for Sb-Te, e.g., 2.97 and 3.30 Å for $Ge_2Sb_2Te_5$ (stable phase), which is very similar to the results obtained for the Sb_2Te_3 rhombohedral structure. However, the existence of several bond lengths for Ge-Te depends on the composition. For example, for $GeSb_2Te_4$ and $GeSb_4Te_7$ there is only one bond length (3.01 Å), which is consistent with EXAFS for $GeSb_2Te_4$.[26] For $Ge_3Sb_2Te_6$ and $Ge_2Sb_2Te_5$, we found two bond lengths for Ge-Te, which is also consistent with the EXAFS results.[26] As discussed above, the intermixing of Ge and Sb atoms in the same plane (3Ge-Te-3Sb rule) plays an important role in order to obtain two bond lengths for Ge-Te. Thus, these results indicate that the Ge and Sb atoms are slightly shifted from their high-symmetry sites in the RS-type structure as are Ge atoms in the distorted RS structure. Therefore, our results support the interpretation provided by Kolobov *et al.*,[4] who suggested that the metastable phase adopts a RS-type structure with the cations and anions slightly shifted from their ideal RS positions.

IV. SUMMARY

In summary, first-principles calculations were performed for GeTe, Sb_2Te_3, and crystalline GST phases. From our calculations and analysis, we obtained important insights into the structure and formation mechanism of the crystalline GST phases. We found that crystalline GST compounds form superlattices composed of blocks formed by mGeTe units inserted into a Sb_2Te_3 unit plus $(n-1)$ single Sb_2Te_3 blocks. We identified that strain energy releases by formation of superlattice structures and by maximizing the number of Te atoms surrounded by three Ge and three Sb atoms (3Ge-Te-3Sb), and Peierls-type bond dimerization, which leads to a sequence of short and long bond lengths that lower the crystal total energy. The intrinsic vacancies form ordered planes perpendicular to the stacking direction, which separate the GST building blocks. Furthermore, we explained the volume expansion of the metastable phase as a consequence of Coulomb repulsion between the Te atoms located in adjacent blocks. Our structure models provide a solid foundation for future exploration of the metastable to amorphous transition.

ACKNOWLEDGMENTS

The work was supported by the U.S. Department of Energy under Contract No. DE-AC36-99GO10337. Computing resources of the National Energy Research Scientific Computing Center were employed, which is supported by DOE under Contract No. DE-AC02-05CH11231.

APPENDIX: LATTICE PARAMETERS AND RELATIVE ENERGY DIFFERENCES VERSUS CUTOFF ENERGY AND NUMBER OF k POINTS

As mentioned in Sec. II, the total energies and equilibrium volumes for all structures were obtained by full relaxation of the volume, shape, and atomic positions in the unit cell by minimizing the stress tensor and the atomic forces. It is well known that the convergence of the stress tensor as a function of the number of basis functions is slower than relative total-energy differences. In addition to that, the crystalline GST compounds are composed of building blocks stacked along of the c axis (conventional hexagonal lattice), in which the individual blocks are bound through long-range Te-Te interactions, which are relatively weaker compared to the Ge-Te bonds. Furthermore, we observe that GST structures with slightly different occupation of the lattice sites by the Ge, Sb, Te, and intrinsic vacancies have very similar energies, e.g., the hexagonal and RS phases differs by few meV/f.u. The most important computational parameters are the cutoff energy and the number of **k** points in the Brillouin zone. Therefore, in order to demonstrate the accuracy of our calculations, which is important to support our conclusions, we report in this Appendix convergence calculations of the equilibrium lattice constants and relative energy differences as a function of the cutoff energy and number of **k** points in the Brillouin zone.

Equilibrium lattice parameters: For those calculations, we employed the $Ge_2Sb_2Te_5$ composition and a (1×1) unit cell as a test case, which contains 3 f.u. stacked along of the c axis (see Fig. 2). Using the stress tensor to optimize equilibrium lattice parameters requires special care, e.g., the initial lattice constants are different from the final ones, however, the G vectors (basis set) were defined for the initial lattice. To avoid such problems, our stress tensor calculations were restarted several times (from three to six times) in order to achieve the convergence requirements. The results for a_0 and c_0 as a function of cutoff energy and number of **k** points in the irreducible part of the Brillouin zone (IBZ) are shown in Figs. 5 and 6. The changes in the lattice parameters are given in percent with respect to the calculations obtained with the largest cutoff energy and largest number of **k** points.

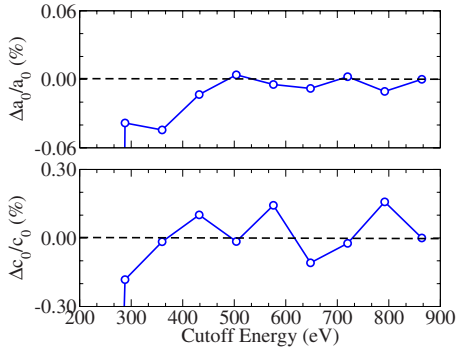

FIG. 5. (Color online) Convergence of the lattice parameters a_0 and c_0 as a function of the plane-wave cutoff energy.

Using a $(6\times6\times1)$ **k**-point grid and a cutoff energy of 288 eV, which is the recommended cutoff energy for total-energy calculations by the VASP developers for systems containing Ge (d states in the valence), Sb, and Te PAW projectors, we found that a_0 and c_0 change by less than 0.04% and 0.20% compared to calculations using a cutoff energy of 864 eV and the same **k**-point grid. Thus, even a relatively small cutoff energy yields quite accurate lattice constants using stress tensor calculations. In order to decrease the relative error in c_0, higher cutoff energies are required. Therefore, in the present work, we employed a cutoff energy of 576 eV, which is 2×288 eV, in order to obtain accurate results for the equilibrium volumes. Using a cutoff energy of 576 eV

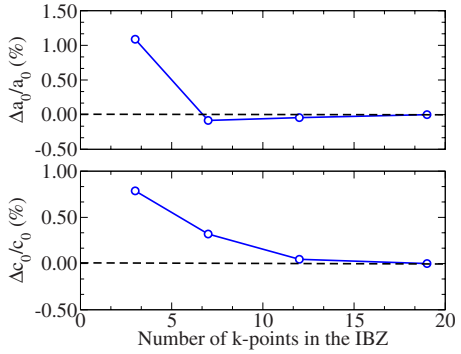

FIG. 6. (Color online) Convergence of the lattice parameters a_0 and c_0 as a function of the number of **k** points in the irreducible part of the Brillouin zone. We employed $(3\times3\times1)$, $(6\times6\times1)$, $(9\times9\times1)$, and $(12\times12\times1)$ **k**-point grids, which yield 3, 7, 12, and 19 **k** points in the IBZ.

and a $(3\times3\times1)$ **k**-point grid (three **k** points in the IBZ), we found that a_0 and c_0 change by 1.09% and 0.79% compared to calculations using a $(12\times12\times1)$ **k**-point grid (19 **k** points in the IBZ). Thus, three **k** points in the IBZ do not provide accurate results. Calculations using a $(6\times6\times1)$ grid (seven **k** points in the IBZ) yields relative errors of 0.08% and 0.32% for a_0 and c_0, respectively. Therefore, taking into account accuracy and computational cost, all stress tensor calculations were performed using a cutoff energy of 576 eV and a $(6\times6\times1)$ **k**-point grid.

Relative energy differences: In order to check the convergence of the relative energy differences between two alternative structures, we calculated the energy difference between the stable and metastable phases of $Ge_2Sb_2Te_5$ as a function of cutoff energy and number of **k** points in the IBZ. Using a cutoff energy of 288 eV and a $(6\times6\times1)$ **k**-point grid, we found that the stable phase (hexagonal structure) is 8.76 meV/f.u. lower in energy than the metastable (RS structure), which increases to 9.30 meV/f.u. using 432 eV and the same **k**-point grid. It changes from 8.76 to 7.98 meV/f.u. by increasing the **k**-point grid from $(6\times6\times1)$ to $(12\times12\times1)$ for a cutoff energy of 288 eV. Thus, for the total-energy calculations for the relative energy differences, we employed a cutoff energy of 288 eV and the same **k**-point grid. The resulting precision in comparing total energies can therefore be estimated at about ±2 meV/f.u.

[1] G. I. Meijer, Science **319**, 1625 (2008).
[2] M. Wuttig and N. Yamada, Nature Mater. **6**, 824 (2007).
[3] S. R. Ovshinsky, Phys. Rev. Lett. **21**, 1450 (1968).
[4] A. V. Kolobov, P. Fons, A. I. Frenkel, A. L. Ankudinov, J. Tominaga, and T. Uruga, Nature Mater. **3**, 703 (2004).
[5] A. V. Kolobov, J. Haines, A. Pradel, M. Ribes, P. Fons, J. Tominaga, Y. Katayama, T. Hammouda, and T. Uruga, Phys. Rev. Lett. **97**, 035701 (2006).
[6] W. Welnic, A. Pamungkas, R. Detemple, C. Steimer, S. Blügel, and M. Wuttig, Nature Mater. **5**, 56 (2006).
[7] J. Akola and R. O. Jones, Phys. Rev. B **76**, 235201 (2007).
[8] D. A. Baker, M. A. Paesler, G. Lucovsky, S. C. Agarwal, and P. C. Taylor, Phys. Rev. Lett. **96**, 255501 (2006).
[9] P. Jóvári, I. Kaban, J. Steiner, B. Beuneu, A. Schöps, and M. A. Webb, Phys. Rev. B **77**, 035202 (2008).
[10] J. Hegedüs and S. R. Elliott, Nature Mater. **7**, 399 (2008).
[11] J.-W. Park *et al.*, Appl. Phys. Lett. **93**, 021914 (2008).
[12] K. A. Agaev and A. G. Talybov, Sov. Phys. Crystallogr. **11**, 400 (1966).
[13] I. I. Petrov, R. M. Imamov, and Z. G. Pinsker, Sov. Phys. Crystallogr. **13**, 339 (1968).
[14] O. G. Karpinsky, L. E. Shelimova, M. A. Kretova, and J.-P. Fleurial, J. Alloys Compd. **268**, 112 (1998).
[15] L. E. Shelimova, O. G. Karpinskii, M. A. Kretova, V. I. Kosyakov, V. A. Shestakov, V. S. Zemskov, and F. A. Kuznetsov, Inorg. Mater. **36**, 768 (2000).
[16] B. J. Kooi and T. T. M. De Hosson, J. Appl. Phys. **92**, 3584 (2002).
[17] T. Matsunaga and N. Yamada, Phys. Rev. B **69**, 104111 (2004).
[18] T. Matsunaga, N. Yamada, and Y. Kubota, Acta Crystallogr., Sect. B: Struct. Sci. **60**, 685 (2004).
[19] T. Matsunaga, R. Kojima, N. Yamada, K. Kifune, Y. Kubota, and M. Takata, Appl. Phys. Lett. **90**, 161919 (2007).
[20] T. Matsunaga *et al.*, J. Appl. Phys. **103**, 093511 (2008).
[21] Z. Sun, J. Zhou, and R. Ahuja, Phys. Rev. Lett. **96**, 055507 (2006).
[22] Z. Sun, S. Kyrsta, D. Music, R. Ahuja, and J. M. Schneider, Solid State Commun. **143**, 240 (2007).
[23] T. Nonaka, G. Ohbayashi, Y. Toriumi, Y. Mori, and H. Hashimoto, Thin Solid Films **370**, 258 (2000).
[24] N. Yamada and T. Matsunaga, J. Appl. Phys. **88**, 7020 (2000).
[25] Y. J. Park, J. Y. Lee, M. S. Youm, Y. T. Kim, and H. S. Lee, J. Appl. Phys. **97**, 093506 (2005).
[26] A. V. Kolobov, P. Fons, J. Tominaga, A. I. Frenkel, A. L. Ankudinov, S. N. Yannopoulos, K. S. Andrikopoulos, and T. Uruga, Jpn. J. Appl. Phys., Part 1 **44**, 3345 (2005).
[27] J. H. Eom, Y. G. Yoon, C. Park, H. Lee, J. Im, D. S. Suh, J. S. Noh, Y. Khang, and J. Ihm, Phys. Rev. B **73**, 214202 (2006).
[28] P. E. Blöchl, Phys. Rev. B **50**, 17953 (1994).
[29] G. Kresse and D. Joubert, Phys. Rev. B **59**, 1758 (1999).
[30] J. P. Perdew, K. Burke, and M. Ernzerhof, Phys. Rev. Lett. **77**, 3865 (1996).
[31] G. Kresse and J. Hafner, Phys. Rev. B **48**, 13115 (1993).
[32] G. Kresse and J. Furthmüller, Phys. Rev. B **54**, 11169 (1996).
[33] J. Goldak, C. S. Barrett, D. Innes, and W. Youdelis, J. Chem. Phys. **44**, 3323 (1966).
[34] T. Chattopadhyay, J. X. Boucherle, and H. G. von Schnering, J. Phys. C **20**, 1431 (1987).
[35] A. Onodera, I. Sakamoto, Y. Fujii, N. Mori, and S. Sugai, Phys. Rev. B **56**, 7935 (1997).
[36] A. V. Kolobov, J. Tominaga, P. Fons, and T. Uruga, Appl. Phys. Lett. **82**, 382 (2003).
[37] A. Ciucivara, B. R. Sahu, and L. Kleinman, Phys. Rev. B **73**, 214105 (2006).
[38] H. M. Polatoglou, G. Theodorou, and N. A. Economou, J. Phys. C **16**, 817 (1983).
[39] J. K. Burdett and S. Lee, J. Am. Chem. Soc. **105**, 1079 (1983).
[40] J.-P. Gaspard, A. Pellegatti, F. Marinelli, and C. Bichara, Philos. Mag. B **77**, 727 (1998).
[41] J.-P. Gaspard and R. Ceolin, Solid State Commun. **84**, 839 (1992).
[42] J. F. Cornwell, *Group Theory and Electronic Energy Bands in Solids* (North-Holland, Amsterdam, 1969).
[43] L. G. Khvostantsev, A. I. Orlov, N. K. Abrikosov, and L. D. Ivanova, Phys. Status Solidi A **89**, 301 (1985).
[44] P. Villars and L. D. Calvert, *Persons's Handbook of Crystallographic Data for Intermetallic Phases* (ASM International, Materials Park, OH, 1991).
[45] M. Fuchs, J. L. F. Da Silva, C. Stampfl, J. Neugebauer, and M. Scheffler, Phys. Rev. B **65**, 245212 (2002).
[46] J. L. F. Da Silva, C. Stampfl, and M. Scheffler, Surf. Sci. **600**, 703 (2006).
[47] J. L. F. Da Silva, S.-H. Wei, J. Zhou, and X. Wu, Appl. Phys. Lett. **91**, 091902 (2007).

[48] T. Thonhauser, T. J. Scheidemantel, J. O. Sofo, J. V. Badding, and G. D. Mahan, Phys. Rev. B **68**, 085201 (2003).
[49] M. Wuttig, D. Lüsebrink, D. Wamwangi, W. Welnic, M. Gillessen, and R. Dronskowski, Nature Mater. **6**, 122 (2007).
[50] G. Lee and S.-H. Jhi, Phys. Rev. B **77**, 153201 (2008).
[51] G. Trimarchi and A. Zunger, Phys. Rev. B **75**, 104113 (2007).
[52] J. L. F. Da Silva, Y. Yan, and S.-H. Wei, Phys. Rev. Lett. **100**, 255501 (2008).
[53] W. K. Njoroge, H.-W. Wöltgens, and M. Wuttig, J. Vac. Sci. Technol. A **20**, 230 (2002).